Experimental Study of a Fuel−Rich Premixed Toluene Flame at Low Pressure

ARTICLE *in* ENERGY & FUELS · MARCH 2009

Impact Factor: 2.79 · DOI: 10.1021/ef800902t

7 AUTHORS, INCLUDING:

Zhen-Yu Tian
Chinese Academy of Sciences
66 PUBLICATIONS **889** CITATIONS
SEE PROFILE

Jing Wang
University of Southampton
910 PUBLICATIONS **9,705** CITATIONS
SEE PROFILE

Bin Yang
University of Oklahoma
29 PUBLICATIONS **805** CITATIONS
SEE PROFILE

Article

Experimental Study of a Fuel-Rich Premixed Toluene Flame at Low Pressure

Yuyang Li, Lidong Zhang, Zhenyu Tian, Tao Yuan, Jing Wang, Bin Yang, and Fei Qi

Energy Fuels, **2009**, 23 (3), 1473-1485• DOI: 10.1021/ef800902t • Publication Date (Web): 10 February 2009

Experimental Study of a Fuel-Rich Premixed Toluene Flame at Low Pressure

Yuyang Li, Lidong Zhang, Zhenyu Tian, Tao Yuan, Jing Wang, Bin Yang,† and Fei Qi*

National Synchrotron Radiation Laboratory, University of Science and Technology of China, Hefei, Anhui 230029, P.R. China

Received October 19, 2008. Revised Manuscript Received December 29, 2008

A low-pressure premixed toluene/O_2/Ar flame with the equivalence ratio of 1.90 was investigated using tunable synchrotron vacuum ultraviolet (VUV) photoionization mass spectrometry. Combustion intermediates up to $C_{19}H_{12}$ were identified by the measurements of the photoionization mass spectrum and photoionization efficiency spectrum. Mole fraction profiles of flame species were evaluated from the scan of burner position at photon energies near ionization thresholds. Furthermore, flame temperature was recorded by a Pt/Pt-13%Rh thermocouple. The comprehensive experimental data concerning the flame structure facilitate the discussion about the flame chemistry of toluene and other monocyclic aromatic fuels. Benzyl and benzene were found to be major primary intermediates of toluene degradation; and benzene is suggested to originate mainly from fuel degradation instead of radical recombination channels in fuel-rich monocyclic aromatic hydrocarbon flames. On the basis of the intermediate identification, comparison is made among the current mechanisms relevant to the formation of polycyclic aromatic hydrocarbons (PAHs). It is concluded that the molecular growth process in this flame is consistent with the synergy of the hydrogen-abstraction-carbon-addition (HACA) mechanism and the resonantly stabilized radical addition mechanism. In particular, the HACA mechanism can connect a great deal of aromatic intermediates observed in the present work and consequently explain the regular ring enlargement by consecutive addition of 2 or 4 carbon atoms, while the resonantly stabilized radical addition mechanism may have marked and sometimes predominant influences on the formation of many typical PAHs.

1. Introduction

Small aromatic hydrocarbons have a number of desirable advantages as fuels, such as a high-energy rating and a high knock rating.[1,2] They are extensively used in gasoline for the improvement of fuel octane number, as well as in diesels and jet fuels. On the other hand, their toxicity and ability to form toxic species during oxidation processes can do harm to human health and environmental security. For example, benzene, toluene, ethylbenzene, and xylenes, known as BTEX, are ubiquitously environmental contaminants and health hazards, leading to human neurological diseases or cancer.[3] Furthermore, it is largely agreed that small aromatics are precursors of polycyclic aromatic hydrocarbons (PAHs),[4] which are well-known to be mutagenic, carcinogenic, and teratogenic.[5,6]

As the simplest substituted aromatic hydrocarbon, toluene is the richest single aromatic component of most practical fuels. For example, its mole fraction can reach as high as 10% in premium fuels. Because of the high octane number, toluene is widely used in the surrogate mixtures of gasolines.[7,8] Additionally, toluene can be formed during the oxidation and pyrolysis of other hydrocarbons and commercial fuels, leading to the formation of larger aromatics like PAHs and eventually soot.[9,10] Thus, the combustion chemistry of toluene is of special interest not only because of its prevalent and extensive use as a practical fuel but also because of its role as the precursor of PAHs and soot. However, the majority of previous experimental investigations were limited to the measurements of global data, such as ignition delay times in shock tubes[11] or in rapid compression machines[12] and laminar flame speeds.[13]

There are a limited number of studies that focused on identification and quantification of intermediate species formed during toluene oxidation and combustion. Barnard and Ibberson investigated the gaseous oxidation of toluene over the temperature range of 450 to 515 °C and reported combustion intermediates including methane, ethylene, benzene, formaldehyde, and benzaldehyde using gas chromatography (GC).[14,15]

* To whom correspondence should be addressed. E-mail: fqi@ustc.edu.cn. Fax: +86-551-5141078. Phone: +86-551-3602125.

† Current Address: School of Applied and Engineering Physics, Cornell University, Ithaca, New York 14850.

(1) Goodger, E.; Vere, R. *Aviations Fuel Technology*; MacMillan Publishers: London, 1985.

(2) *ASTM Special Technical Publication No. 225*; American Society of Testing Materials: Philadelphia, 1958.

(3) Chiou, C. T.; Schmedding, D. W.; Manes, M. *Environ. Sci. Technol.* **1982**, *16*, 4–10.

(4) Frenklach, M. *Phys. Chem. Chem. Phys.* **2002**, *4*, 2028–2037.

(5) Marr, L. C.; Kirchstetter, T. W.; Harley, R. A.; Miguel, A. H.; Hering, S. V.; Hammond, S. K. *Environ. Sci. Technol.* **1999**, *33*, 3091–3099.

(6) Luch, A. *The Carcinogenic Effects of Polycyclic Aromatic Hydrocarbons*; Imperial College Press: London, 2005.

(7) Humer, S.; Frassoldati, A.; Granata, S.; Faravelli, T.; Ranzi, E.; Seiser, R.; Seshadri, K. *Proc. Combust. Inst.* **2007**, *31*, 393–400.

(8) Yahyaoui, M.; Djebaïli-Chaumeix, N.; Dagaut, P.; Paillard, C.-E.; Gail, S. *Proc. Combust. Inst.* **2007**, *31*, 385–391.

(9) Melton, T. R.; Inal, F.; Senkan, S. M. *Combust. Flame* **2000**, *121*, 671–678.

(10) Lindstedt, P.; Maurice, L.; Meyer, M. *Faraday Discuss.* **2002**, *119*, 409–432.

(11) Burcat, A.; Farmer, R. C.; Espinoza, R. L.; Matula, R. A. *Combust. Flame* **1979**, *36*, 313–316.

(12) Roubaud, A.; Minetti, R.; Sochet, L. R. *Combust. Flame* **2000**, *121*, 535–541.

(13) Davis, S. G.; Wang, H.; Brezinsky, K.; Law, C. K. *Proc. Combust. Inst.* **1996**, *26*, 1025–1033.

(14) Barnard, J. A.; Ibberson, V. J. *Combust. Flame* **1965**, *9*, 81–87.

(15) Barnard, J. A.; Ibberson, V. J. *Combust. Flame* **1965**, *9*, 149–157.

10.1021/ef800902t CCC: $40.75
Published on Web 02/10/2009

Brezinsky et al. studied the high-temperature gas-phase oxidation of toluene in a turbulent flow reactor, and the corresponding chemical mechanism as well.[16,17] They measured the mole fraction profiles of intermediates up to $C_{14}H_{14}$ (bibenzyl) during the oxidation processes using GC and gas chromatography/mass spectroscopy (GC/MS). Pamidimukkala et al. performed shock-tube investigations on the high-temperature pyrolysis of toluene, and measured the density gradient and mass spectral product profiles.[18] Dagaut et al. investigated toluene oxidation in a jet-stirred reactor at atmospheric pressure and obtained concentration profiles of 19 molecular species.[19] Sivaramakrishnan et al. performed an experimental study of high-pressure and high-temperature shock-tube oxidation of toluene.[20] On the basis of measured species profiles, they proposed a high-pressure reaction kinetic model to predict the oxidation of toluene in the high temperature region (1200−1500 K).[21] More recently, Bounaceur et al. studied the low-temperature oxidation of toluene in a continuous flow stirred tank reactor and provided the mole fraction profiles of 17 species by GC.[22] On the basis of these experimental studies, kinetic modeling studies were carried out to increase the knowledge of the combustion mechanism of toluene. Detailed kinetic models of toluene oxidation were reported by many groups, including Emdee et al.,[23] Colket and Seery,[24] Lindstedt and Maurice,[25] Dagaut et al.,[19] and Bounaceur et al.[22]

It should be mentioned that to date the detailed chemical structures of intermediate species are scarcely studied for toluene combustion, especially for premixed flames. Only two groups have studied the premixed flames of toluene. In 2005, Zervas investigated the toluene/isooctane flames with near stoichiometric equivalence ratios and observed a series of oxygenated compounds, including carbonyl compounds, alcohols, and organic acids.[26] On the basis of the measured concentration profiles, he concluded that the concentrations of these oxygenated intermediates are strongly dependent on the air/fuel ratios; that is, fuel-lean and stoichiometric conditions could lead to larger concentrations of oxygenated compounds than fuel-rich conditions. El Bakali et al. examined toluene degradation in a low-pressure stoichiometric premixed methane/toluene flame.[27] Using electron-impact mass spectrometry (EIMS), they measured mole fraction profiles for more than 30 flame species and adopted a detailed mechanism to model the experimental data. Therefore, the lack of flame data for toluene has greatly limited our understanding of combustion chemistry of monocyclic aromatic fuels and formation mechanism of PAHs and soot.

Here, we report an experimental study of a fuel-rich toluene/O_2/Ar flame ($\phi = 1.90$, C/O = 0.74) at 30.0 torr with molecular-beam mass spectrometry (MBMS). The tunable synchrotron VUV photoionization is employed in this study, which uses a single-photon ionization method and can realize the isomeric identification of flame species.[28] The present work aims to report experimental data of the monocyclic aromatic hydrocarbon combustion that can enrich the database for modeling studies. On the basis of the intermediate identification and mole fraction measurement in this flame, the flame chemistry involving the primary degradation of toluene and the formation of large aromatics and PAHs is discussed. Modeling studies based on the experimental results will be reported in future.

2. Experimental Section

2.1. Instruments. The experimental work was carried out at the flame endstation of the National Synchrotron Radiation Laboratory (NSRL) in Hefei, China. As reported elsewhere,[28−30] the experimental setup of synchrotron VUV photoionization mass spectrometry consists of a flame chamber, a differentially pumped chamber with a molecular-beam sampling system, and a photoionization chamber with a reflectron time-of-flight mass spectrometer (RTOF-MS).[31] A 6.0 cm-diameter McKenna burner is located at the center of the flame chamber, and a laminar premixed flame is stabilized on its surface. A quartz cone-like nozzle with a 40° included angle and a ~500 μm orifice at the tip is used to sample the flame species which can form a molecular beam in the differentially pumped chamber and pass into the photoionization chamber through a nickel skimmer. The molecular beam is crossed by the tunable synchrotron VUV light in the ionization region. Then the photoions are collected and analyzed by the RTOF-MS with an approximate mass resolving power of 1,400 and an estimated detection limit of 1 ppm.

Two beamlines were used for this study. One is a newly constructed beamline using undulator radiation from the 800 MeV electron storage ring. Synchrotron radiation is dispersed by a 1m Seya-Namioka monochromator equipped with a 1,500 grooves/mm grating covering the photon energies from 7.8 to 24 eV. A gas filter was used to eliminate higher-order harmonic radiation with Ne or Ar filled in the gas cell. The energy resolving power ($E/\Delta E$) is around 1000, and the average photon flux can reach the magnitude of 10^{13} photons/sec. Another one is a bending magnet beamline which has been described in detail in our previous studies.[29,32] A LiF window is used to eliminate the high-order harmonic radiation when the photon energy is lower than 11.8 eV (105 nm). Most experiments were carried out at the undulator beamline, and the measurement of photoionization efficiency (PIE) spectrum at photon energy ranging from 6.8 to 11.8 eV was performed at the bending magnet beamline.

2.2. Flame Conditions. Toluene was purchased from Sinopharm Chemical Reagent Limited Co., Shanghai, China, with a purity of ≥99.5%. A syringe pump (ISCO 1000D, U.S.A.) was used to control the liquid flow rate of 1.000 ± 0.005 mL/min at room temperature. The gas flow rates of O_2 and Ar were 0.997 ± 0.005 and 0.900 ± 0.005 standard liters per minute (SLM), respectively, which were controlled separately by mass flow controllers (MKS, U.S.A.). Thus, the equivalence ratio of this flame is 1.90 ± 0.02 and the mass flow rate of the reagent mixture is (2.30 ± 0.01) × 10^{-3} g/(sec·cm^2). In this work, the flame was stabilized at 30.0 torr (4.00 kPa), and the inlet cold-

(16) Brezinsky, K.; Litzinger, T. A.; Glassman, I. *Int. J. Chem. Kinet.* **1984**, *16*, 1053–1074.
(17) Brezinsky, K. *Prog. Energy Combust. Sci.* **1986**, *12*, 1–24.
(18) Pamidimukkala, K. M.; Kern, R. D.; Patel, M. R.; Wei, H. C.; Kiefer, J. H. *J. Phys. Chem.* **1987**, *91*, 2148–2154.
(19) Dagaut, P.; Pengloan, G.; Ristori, A. *Phys. Chem. Chem. Phys.* **2002**, *4*, 1846–1854.
(20) Sivaramakrishnan, R.; Tranter, R. S.; Brezinsky, K. *Combust. Flame* **2004**, *139*, 340–350.
(21) Sivaramakrishnan, R.; Tranter, R. S.; Brezinsky, K. *Proc. Combust. Inst.* **2005**, *30*, 1165–1173.
(22) Bounaceur, R.; Da Costa, I.; Fournet, R.; Billaud, F.; Battin-Leclerc, F. *Int. J. Chem. Kinet.* **2005**, *37*, 25–49.
(23) Emdee, J. L.; Brezinsky, K.; Glassman, I. *J. Phys. Chem.* **1992**, *96*, 2151–2161.
(24) Colket, M. B.; Seery, D. J. *Proc. Combust. Inst.* **1994**, *25*, 883–892.
(25) Lindstedt, R. P.; Maurice, L. Q. *Combust. Sci. Technol.* **1996**, *120*, 119–167.
(26) Zervas, E. *Energy Fuels* **2005**, *19*, 1865–1872.
(27) El Bakali, A.; Dupont, L.; Lefort, B.; Lamoureux, N.; Pauwels, J. F.; Montero, M. *J. Phys. Chem. A* **2007**, *111*, 3907–3921.
(28) Qi, F.; Yang, R.; Yang, B.; Huang, C. Q.; Wei, L. X.; Wang, J.; Sheng, L. S.; Zhang, Y. W. *Rev. Sci. Instrum.* **2006**, *77*, 084101.
(29) Yang, B.; Li, Y. Y.; Wei, L. X.; Huang, C. Q.; Wang, J.; Tian, Z. Y.; Yang, R.; Sheng, L. S.; Zhang, Y. W.; Qi, F. *Proc. Combust. Inst.* **2007**, *31*, 555–563.
(30) Yang, B.; Oβwald, P.; Li, Y. Y.; Wang, J.; Wei, L. X.; Tian, Z. Y.; Qi, F.; Kohse-Hoinghaus, K. *Combust. Flame* **2007**, *148*, 198–209.
(31) Huang, C. Q.; Yang, B.; Yang, R.; Wang, J.; Wei, L. X.; Shan, X. B.; Sheng, L. S.; Zhang, Y. W.; Qi, F. *Rev. Sci. Instrum.* **2005**, *76*, 126108.
(32) Li, Y. Y.; Huang, C. Q.; Wei, L. X.; Yang, B.; Wang, J.; Tian, Z. Y.; Zhang, T. C.; Sheng, L. S.; Qi, F. *Energy Fuels* **2007**, *21*, 1931–1941.

flow (273 K) velocity is calculated to be 31.5 ± 0.2 cm/sec. The temperature profile was measured using a Pt/Pt-13%Rh thermocouple of 0.076 mm in diameter, coated with Y_2O_3−BeO anti-catalytic ceramic to avoid the catalytic effects.[33] The thermocouple was located at 20 mm upstream of the quartz nozzle, and the bead at the axial direction of the burner. Radiative heat losses have been considered and calibrated to the temperature profile.[34] On the basis of the reproducibility of temperature measurement, the uncertainty of the maximum flame temperature was estimated to be ±100 K. Furthermore, previous studies indicated that the cooling effect of the quartz nozzle could result in the reduction of the flame temperature by approximately 100 K in the high temperature region.[35,36]

2.3. Data Analysis Methods. The experimental results are recorded in the photoionization mass spectra. A mass spectrum can only provide the information on mass distribution of ionized flame species. Two measurement procedures are adopted in premixed flame studies using synchrotron VUV photoionization mass spectrometry. With the variation of photon energy, a series of mass spectra can be measured in the middle of the luminous flame region (7.5 mm from the burner surface in this work), where most combustion intermediates have high concentrations. The integrated ion signals for a specific mass are normalized by photon flux and plotted versus the photon energy, which can yield a PIE spectrum containing precise information of the ionization energies (IEs) of corresponding species. Considering the cooling effect of the molecular beam,[37] the errors of IE determination are ±0.05 eV for species with strong signal-to-noise (S/N) ratios and ±0.10 eV for species with poor S/N ratios.

To obtain the spatial distribution of flame species, the burner is driven by a step motor to move toward or away from the quartz nozzle, which makes it possible to take mass spectra at different flame positions. To keep near-threshold ionization and avoid fragmentation, we scanned the burner position at several selected photon energies. Similarly to the measurement of PIE spectra, the spatial plots of integrated ion signals versus the burner position can be deduced from the raw data. According to the evaluation method described in the Supporting Information, mole fraction profiles of flame species can be determined from the scan of burner position. The evaluation method is developed from literature methods[38−41] and has been applied in our previous studies.[42,43] In brief, the signal of flame species i is concluded as a function of the photon energies E and the position that is represented by the local flame temperature T,

$$S_i(T,E) = CP_i(T)\,\sigma_i(E)\,D_i\Phi_p(E)\,F(k,T,P) \quad (1)$$

where C is a constant and P is the pressure of the flame chamber; $P_i(T)$ is the species partial pressure at the sampling position and corresponds to the mole fraction of species i, $X_i(T)$; $\sigma_i(E)$ is the photoionization cross section at the photon energy E; D_i is the mass discrimination factor for species i; $\Phi_p(E)$ is the photon flux; $F(k,T,P)$ is an empirical instrumental sampling function, which depends on bulk properties of the flame sample and is the same for all flame species, and k is the specific heat ratio. The measurement of mass discrimination factor and determination of photoionization cross section are also presented in the Supporting Information. Considering errors of signal reproduction, photoionization cross sections, mass discrimination factors, and the evaluation method itself, the determined mole fractions should have uncertainties of within ±10% for major species, ±25% for combustion intermediates with accurately known photoionization cross sections, and a factor of 2 for those with estimated photoionization cross sections.

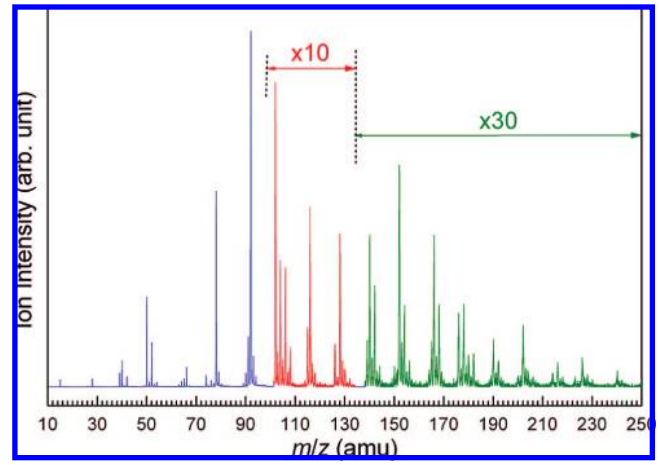

Figure 1. Mass spectrum of the premixed toluene/O_2/Ar flame (ϕ = 1.90) taken at the photon energy of 10.80 eV and the burner position of 7.5 mm. Partial mass regions are amplified by 10 or 30 times for clear display.

3. Results and Discussions

3.1. Identification of Combustion Intermediates. The identification of combustion intermediates is a key step to understand the flame chemistry. However, flame is an extremely complex chemical system with hundreds of combustion intermediates; and many intermediates are isomeric species and reactive radicals. Figure 1 displays a mass spectrum of this flame taken at the photon energy of 10.8 eV and the burner position of 7.5 mm, in which a great number of mass peaks can be observed. Hence, to achieve comprehensive identification of combustion intermediates, the detection procedure should have low fragmental interference, high detection sensitivity, isomeric discriminability, and radical detectability. Synchrotron VUV photoionization combined with MBMS can satisfy these requirements because of the high photon flux, single-photon ionization process, and wavelength tunability in the VUV region, making it a selective and sensitive diagnostic tool in flame chemistry research.[44]

Identification of combustion intermediates by synchrotron VUV photoionization is mainly based on the accordance of measured ionization thresholds (deflections on a PIE spectrum) and literature IEs, which can help find out the dominant intermediates for the observed mass peak. Minor intermediates do exist, but their concentrations are too low to be detected by this and other techniques. Literature IEs of most combustion intermediates can be obtained from the NIST online database[45]

(33) Kent, J. H. *Combust. Flame* **1970**, *14*, 279–281.
(34) Fristrom, R. M. *Flame Structure and Processes*; Oxford: New York, 1995.
(35) Desgroux, P.; Gasnot, L.; Pauwels, J. F.; Sochet, L. R. *Appl. Phys. B: Laser Opt.* **1995**, *61*, 401–407.
(36) Gueniche, H. A.; Glaude, P. A.; Dayma, G.; Fournet, R.; Battin-Leclerc, F. *Combust. Flame* **2006**, *146*, 620–634.
(37) Kamphus, M.; Liu, N. N.; Atakan, B.; Qi, F.; McIlroy, A. *Proc. Combust. Inst.* **2002**, *29*, 2627–2633.
(38) Bhargava, A.; Westmoreland, P. R. *Combust. Flame* **1998**, *113*, 333–347.
(39) Cool, T. A.; Nakajima, K.; Taatjes, C. A.; McIlroy, A.; Westmoreland, P. R.; Law, M. E.; Morel, A. *Proc. Combust. Inst.* **2005**, *30*, 1681–1688.
(40) Defoeux, F.; Dias, V.; Renard, C.; Van Tiggelen, P. J.; Vandooren, J. *Proc. Combust. Inst.* **2005**, *30*, 1407–1415.
(41) Wang, J.; Yang, B.; Cool, T. A.; Hansen, N.; Kasper, T. *Int. J. Mass Spectrom.* **2008**, *269*, 210–220.
(42) Li, Y. Y.; Tian, Z. Y.; Zhang, L. D.; Tuan, T.; Zhang, K. W.; Yang, B.; Qi, F. *Proc. Combust. Inst.* **2009**, *32*, 647−655.
(43) Li, Y. Y.; Zhang, L. D.; Tian, Z. Y.; Tuan, T.; Zhang, K. W.; Yang, B.; Qi, F. *Proc. Combust. Inst.* **2009**, *32*, 1293−1300.
(44) McEnally, C. S.; Pfefferle, L. D.; Atakan, B.; Kohse-Hoinghaus, K. *Prog. Energy Combust. Sci.* **2006**, *32*, 247–294.
(45) Linstrom, P. J.; Mallard, W. G. *NIST Chemistry Webbook*, Number 69; National Institute of Standard and Technology: Gaithersburg, MD, 2005; http://webbook.nist.gov.

Table 1. Calculation Results of Ionization Energies (IEs) of Aromatic Intermediates

Formula	Name	Structure	IE/eV	Method	Formula	Name	Structure	IE/eV	Mehod
C_7H_6	phenylmethylene		5.98	G3B3	$C_{16}H_{12}$	1-phenyl naphthalene	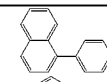	7.61	DFT+MP2
	5-ethenylidene-1,3-cyclopentadiene		8.26	G3B3	$C_{17}H_{12}$	7H-benzo[de] anthracene	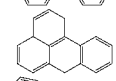	7.24	DFT+MP2
	bicyclo[4.1.0]hepta-1,3,5-triene		8.84	G3B3		benzo[a]fluorene	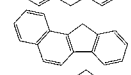	7.32	DFT+MP2
C_9H_{10}	indane		8.54	G3B3		benzo[b]fluorene	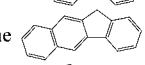	7.32	DFT+MP2
C_9H_6O	inden-1-one		8.67	DFT+MP2		benzo[c]fluorene	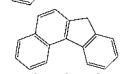	7.37	DFT+MP2
$C_{12}H_6$	1,2-dehydro acenaphthylene		8.53	G3B3	$C_{19}H_{12}$	3H-benzo [cd]pyrene	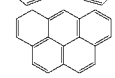	6.67	DFT+MP2
	1,3,5-triethynyl benzene	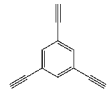	8.93	G3B3		11H-benz[bc] aceanthrylene	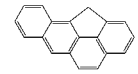	7.06	DFT+MP2
$C_{13}H_{10}$	phenalene		7.37	DFT+MP2		1-ethylnyl benzo[a]fluorene	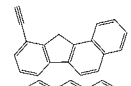	7.21	DFT+MP2
$C_{15}H_{10}$	cyclopropa[b] anthracene	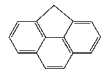	7.68	DFT+MP2		a-$C_{19}H_{12}$	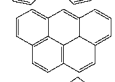	7.25	DFT+MP2
$C_{16}H_{10}$	aceanthrylene	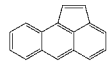	7.22	DFT+MP2		4H-cyclopenta [def]chrysene	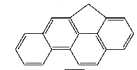	7.35	DFT+MP2
	acephenanthrylene	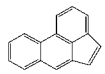	7.81	DFT+MP2		4H-cyclopenta [def]triphenylene	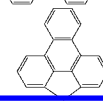	7.59	DFT+MP2

and many previous computational studies.[29,46−48] Besides, species with unknown or ambiguous IE may exist in combustion process. Therefore for these species, the geometries and harmonic vibrational frequencies of neutral molecules and their corresponding cations were calculated using the GAUSSIAN03 suite of programs.[49] For molecules like C_7H_6, C_9H_{10}, and $C_{12}H_6$, a high level theoretical method, the G3B3 method,[50] was used for geometry optimization and energy calculations. However, the G3B3 method is quite time-consuming and is unable to process molecules with complex structure. Hence a B3LYP method[51] with the 6-311G(d,p) basis set was used for geometry optimization and frequency calculation for these molecules. Single point energy calculation was performed with a combination of B3LYP/6-31++G(2df,p) and MP2/6-31+G(2df,p) methods, which has been verified to have higher accuracy than either B3LYP or MP2 method.[52] Therefore, accurate energies were calculated using the following equation[52]

$$E[\text{B3LYP/6-31++G(2df,p)} + \text{MP2/6-31+G(2df,p)}] \approx (E[\text{B3LYP/6-31++G(2df,p)}] + E[\text{MP2/6-31+G(2df,p)}]) \times 0.5 + \text{Zero Point Energy} \times 0.9614 \quad (2)$$

The calculation results are summarized in Table 1, along with the molecular structures and calculation methods.

The PIE spectra of many small hydrocarbon intermediates have been reported in our previous studies.[29,30,32,53] Therefore in this section, the identification of some typical PAHs will be presented in detail. Figure 2 displays four PIE spectra of PAHs with increasing carbonic rings. From Figure 2A, only a threshold at 8.18 eV can be observed for $m/z = 128$, which can be ascribed to the photoionization of naphthalene (IE = 8.14 eV[45]). Figure 2B shows the PIE spectrum of $m/z = 178$, from which two thresholds can be determined. The lower one at 7.46 eV corresponds to the photoionization of anthracene (IE = 7.44 eV[45]), while the higher one at 7.90 eV is consistent with the IE of phenanthrene (7.89 eV[45]). Hence, anthracene and phenanthrene can be identified as the dominant intermediates of $m/z = 178$. For $m/z = 202$, the threshold at 7.47 eV is in good accordance with the IE of pyrene (7.43 eV[45]), while the known IEs of other isomers are either smaller than 7.30 eV or larger than 7.60 eV. Figure 2D presents the PIE spectrum of $m/z = 240$ with a clear threshold at 7.41 eV. But no literature IE is available for its isomers. Hence, we calculated the IE values of many possible $C_{19}H_{12}$ species, as listed in Table 1. Among them,

(46) Hansen, N.; Klippenstein, S. J.; Taatjes, C. A.; Miller, J. A.; Wang, J.; Cool, T. A.; Yang, B.; Yang, R.; Huang, C. Q.; Wang, J.; Qi, F.; Law, M. E.; Westmoreland, P. R. *J. Phys. Chem. A* **2006**, *110*, 3670–3678.

(47) Yang, B.; Huang, C. Q.; Wei, L. X.; Wang, J.; Sheng, L. S.; Zhang, Y. W.; Qi, F.; Zheng, W. X.; Li, W. K. *Chem. Phys. Lett.* **2006**, *423*, 321–326.

(48) Hansen, N.; Klippenstein, S. J.; Westmoreland, P. R.; Kasper, T.; Kohse-Höinghaus, K.; Wang, J.; Cool, T. A. *Phys. Chem. Chem. Phys.* **2008**, *10*, 366–374.

(49) Frisch, M. J.; Trucks, G. W.; Schlegel, H. B.; Scuseria, G. E.; Robb, M. A.; Cheeseman, J. R.; Montgomery, J. A., Jr.; Vreven, T.; Kudin, K. N.; Burant, J. C.; Millam, J. M.; Iyengar, S. S.; Tomasi, J.; Barone, V.; Mennucci, B.; Cossi, M.; Scalmani, G.; Rega, N.; Petersson, G. A.; Nakatsuji, H.; Hada, M.; Ehara, M.; Toyota, K.; Fukuda, R.; Hasegawa, J.; Ishida, M.; Nakajima, T.; Honda, Y.; Kitao, O.; Nakai, H.; Klene, M.; Li, X.; Knox, J. E.; Hratchian, H. P.; Cross, J. B.; Bakken, V.; Adamo, C.; Jaramillo, J.; Gomperts, R.; Stratmann, R. E.; Yazyev, O.; Austin, A. J.; Cammi, R.; Pomelli, C.; Ochterski, J. W.; Ayala, P. Y.; Morokuma, K.; Vot, G. A.; Salvador, P.; Dannenberg, J. J.; Zakrzewski, V. G.; Dapprich, S.; Daniels, A. D.; Strain, M. C.; Farkas, O.; Malick, D. K.; Rabuck, A. D.; Raghavachari, K.; Foresman, J. B.; Ortiz, J. V.; Cui, Q.; Baboul, A. G.; Clifford, S.; Cioslowski, J.; Stefanov, B. B.; Liu, G.; Liashenko, A.; Piskorz, P.; Komaromi, I.; Martin, R. L.; Fox, D. J.; Keith, T.; Al-Laham, M. A.; Peng, C. Y.; Nanayakkara, A.; Challacombe, M.; Gill, P. M. W.; Johnson, B.; Chen, W.; Wong, M. W.; Gonzalez, C.; Pople, J. A. *GAUSSIAN03*, Revision C.02; Gaussian Inc.: Wallingford, CT, 2004.

(50) Baboul, A. G.; Curtiss, L. A.; Redfern, P. C. *J. Chem. Phys.* **1999**, *110*, 7650–7657.

(51) Becke, A. D. *J. Chem. Phys.* **1993**, *98*, 5648–5652.

(52) Wolken, J. K.; Yao, C. X.; Turecek, F.; Polce, M. J.; Wesdemiotis, C. *Int. J. Mass Spectrom.* **2007**, *267*, 30–42.

(53) Huang, C. Q.; Wei, L. X.; Yang, B.; Wang, J.; Li, Y. Y.; Sheng, L. S.; Zhang, Y. W.; Qi, F. *Energy Fuels* **2006**, *20*, 1505–1513.

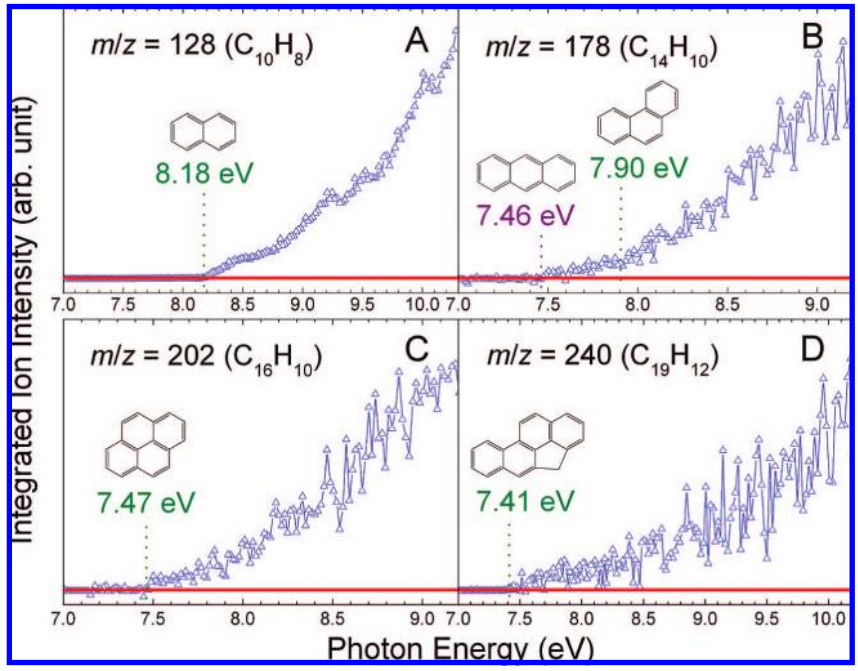

Figure 2. PIE spectra of (A) $m/z = 128$ ($C_{10}H_8$), (B) $m/z = 178$ ($C_{14}H_{10}$), (C) $m/z = 202$ ($C_{16}H_{10}$), and (D) $m/z = 240$ ($C_{19}H_{12}$). Solid lines are used to display the zero point of *Y* axes. The identified species are indicated above the observed ionization thresholds.

4*H*-cyclopenta[def]chrysene is the only one with IE (7.35 eV) close to the measured threshold. Thus, this pentacyclic PAH is assigned as the dominant $C_{19}H_{12}$ species in this flame.

About 100 combustion intermediates from $m/z = 15$ up to 240 were identified in this work and are listed in Table 2 along with their literature/calculated and measured IEs. A series of radicals are identified in this work, including CH_3, C_2H_3, C_2H_5, C_3H_2, C_3H_3, C_3H_5, C_4H_3, C_4H_5, C_5H_3, C_5H_5, C_6H_5, C_7H_7, C_8H_9, and C_9H_7. However, it is difficult to detect the most reactive radicals by MBMS technique, such as H, O, OH, CH, and CH_2, probably because of the heterogeneous recombination of these energetic radicals on the surface of the quartz nozzle.[54,55] Some approximations can be adopted to estimate the concentrations of H, O, and OH radicals, for example, using the partial equilibrium approximation at the end of measured flame region. From an experimental point of view, this problem can be resolved by supplementing the MBMS detection with non-intrusive laser-based optical diagnostics, for example, laser-induced fluorescence (LIF) and cavity ring-down spectroscopy (CRDS).

It is also noted that oxygenated intermediates up to benzaldehyde and benzyl alcohol can be clearly identified, while large ones are still blended with hydrocarbon intermediates. This phenomenon originates from two reasons. First, the direct separation of large oxygenated intermediates and hydrocarbon intermediates from a mass spectrum requires a mass spectrometer with higher mass resolving power. For example, the mass difference between C_9H_{10} ($m/z = 118.1757$) and C_8H_6O ($m/z = 118.1326$) is only 0.0431 atomic mass unit (amu); thus, the separation requires a minimum mass resolving power of 2750 which is twice as that of our mass spectrometer. Second, the IEs of large oxygenated intermediates are always close to those of hydrocarbon intermediates, making it difficult to distinguish the two kinds of molecules via the IE measurement. Therefore, the best solution is to improve the mass resolving power of the mass spectrometer (to a quantity of more than 4000) and reveal these bimodal signal peaks on the mass spectrum.

(54) Hartlieb, A. T.; Atakan, B.; Kohse-Hoinghaus, K. *Combust. Flame* **2000**, *121*, 610–624.

(55) Knuth, E. L. *Combust. Flame* **1995**, *103*, 171–180.

3.2. Flame Chemical Structure. *3.2.1. Mole Fraction Profiles and Temperature Profiles.* Figures 3−9 present the mole fraction profiles of flame species. Symbols represent the measured mole fractions, and B-spline curves are used to connect the symbols and extrapolate the profiles to 0 mm to guide the eye. The maximum mole fractions and peak positions of combustion intermediates, including hydrocarbons, oxygenated hydrocarbons, and radicals, are listed in Table 2. To simplify the figures, mole fraction profiles of the intermediates with the same or close molecular weight will not be displayed separately, and a total mole fraction profile of them will be shown instead.

In the fuel-rich hydrocarbon flames, the fuel, oxidizer, inert species (Ar in this work), and final products (CO_2, CO, H_2O, and H_2) have the highest concentrations and can be called as the major flame species. As seen from their mole fraction profiles shown in Figure 3, toluene is almost burnt out at 10.5 mm, and the oxygen concentration decreases to 0 at 12.0 mm. Hence, the reaction zone of this flame is located before 12 mm, where the fuel decomposes gradually and combustion intermediates react actively with each other. The region beyond 12 mm belongs to the post-flame zone, where the final products are the dominant flame species. The mole fraction profiles of H_2, H_2O, CO, and CO_2 increase quickly in the reaction zone and keep almost invariable at the post-flame zone, indicating that the whole system reaches a nearly equilibrium state in this region. The temperature profile is presented as a solid line in Figure 3.

The mole fraction profiles of combustion intermediates are presented in Figures 4−9, from which some general phenomena can be concluded. First, most intermediates reach their maximum concentrations in the highest temperature region, for example, from 5 to 10 mm in this flame. Second, the mole fraction profiles of oxygenated intermediates peak relatively close to the burner surface in comparison with those of the hydrocarbon intermediates. In this flame, the positions of maximum mole fractions range from 3.5 to 7.5 mm for the oxygenated intermediates and from 5.5 to 9.5 mm for the hydrocarbon intermediates. Furthermore, for the hydrocarbon intermediates with the same

Table 2. List of Combustion Intermediates Measured in This Flame, along with Their IEs, Peak Positions, and Maximum Mole Fractions (X_{MAX}); the Chemical Structures Are Illustrated for Flame Species Heavier than 1,3-Cyclohexadiene

Species				IE (eV)		Mole Fraction	
Mass	Formula	Name	Chemical Structure	Literature [a]	Measured [b]	Peak Position (mm)	X_{MAX}
15	CH_3	methyl radical		9.84	9.86	8.0	1.2E-03
16	CH_4	methane		12.61	12.65	8.5	4.2E-03
26	C_2H_2	acetylene		11.40	11.42	9.5	3.8E-02
27	C_2H_3	vinyl radical		8.59	8.61	8.0	2.5E-05
28	C_2H_4	ethylene		10.51	10.54	8.5	1.5E-03
29	C_2H_5	ethyl radical		8.26	8.30	7.0	2.4E-05
30	C_2H_6	ethane		11.52	11.55	6.5	1.7E-03
30	H_2CO	formaldehyde		10.88	10.93	5.5	4.8E-04
38	C_3H_2	triplet propargylene		8.96	9.04	8.5	3.2E-04
39	C_3H_3	propargyl radical		8.67	8.68	8.5	2.8E-03
40	C_3H_4	propyne		10.36	10.41	7.5	4.7E-04
		allene		9.69	9.75	7.5	1.5E-04
41	C_3H_5	allyl radical		8.14	8.15	8.0	6.9E-05
42	C_2H_2O	ketene		9.62	9.61	7.5	9.5E-04
50	C_4H_2	diacetylene		10.17	10.18	8.5	4.4E-03
51	C_4H_3	CH_2CCCH (i-C_4H_3)		8.06 [c]	8.06	8.5	6.3E-05
52	C_4H_4	vinylacetylene		9.58	9.59	7.5	7.7E-04
		1,2,3-butatriene		9.15	9.14	7.5	1.2E-04
		cyclobutadiene		8.16	8.24	7.0	1.7E-05 [d]
		methylenecyclopropene		8.15			
53	C_4H_5	1-butyn-3-yl radical		7.97 [c]	7.96	6.5	4.0E-05 [d]
		but-2-yn-1-yl radical		7.95 [c]			
54	C_4H_6	1,3-butadiene		9.07	9.10	7.0	2.5E-04
63	C_5H_3	HCCCHCCH (n-C_5H_3)		8.32 [e]	8.25	8.5	4.1E-04
64	C_5H_4	1,3-pentadiyne		9.50	9.54	7.5	1.8E-04
		1,2,3,4-pentatetraene		8.67	8.70	8.0	7.9E-05
65	C_5H_5	cyclopentadienyl radical		8.41	8.45	7.5	1.2E-03
		pent-1-en-4-yn-3-yl radical		7.88	7.86	8.0	1.9E-04
66	C_5H_6	1,3-cyclopentadiene		8.57	8.59	7.0	4.7E-03
74	C_6H_2	1,3,5-hexatriyne		9.50	9.50	8.5	1.1E-03
76	C_6H_4	3-hexene-1,5-diyne		9.07	9.08	8.0	5.2E-04 [d]
		benzyne		9.03			
77	C_6H_5	phenyl radical		8.32	8.35	7.5	3.4E-05
78	C_6H_6	benzene		9.24	9.25	7.5	3.9E-03
		fulvene		8.36	8.40	6.5	4.9E-04
80	C_6H_8	1,3-cyclohexadiene		8.25	8.20	5.5	1.1E-03
88	C_7H_4	1,2-heptadien-4,6-diyne		8.82 [f]	8.83	8.0	2.3E-05
90	C_7H_6	5-ethenylidene-1,3-cyclopentadiene	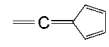	8.26 [g]	8.27	7.5	6.3E-04
91	C_7H_7	benzyl radical		7.24	7.25	7.5	1.2E-03
92	C_7H_8	toluene		8.83	8.85		fuel
		5-methylene-1,3-cyclohexadiene		7.90	7.93	5.5	4.4E-04
94	C_6H_6O	phenol		8.49	8.50	6.0	6.0E-04
98	C_8H_2	1,3,5,7-octatetrayne		9.09	9.16	9.0	8.7E-05
100	C_8H_4	vinylhexatriyne (l-C_8H_4)		8.78 [f]	8.77	8.0	2.0E-05 [d]
		3-octen-1,5,7-triyne (3-C_8H_4)		8.77 [f]			
102	C_8H_6	phenylacetylene		8.82	8.85	8.0	1.4E-03
		benzocyclobutadiene		7.50	7.57	8.0	2.2E-05

Table 2. Countinued

Mass	Formula	Species: Name	Species: Chemical Structure	IE (eV): Literature [a]	IE (eV): Measured [b]	Mole Fraction: Peak Position (mm)	Mole Fraction: X_{MAX}
104	C_8H_8	styrene		8.46	8.47	7.5	5.4E-04
		benzocyclobutene		7.67	7.71	7.5	5.3E-05
105	C_8H_9	4-methylbenzyl radical		6.96	6.95	7.5	1.5E-05 [d]
		1-phenylethyl radical		6.90			
106	C_7H_6O	benzaldehyde		9.50	9.47	3.5	3.8E-04
	C_8H_{10}	ethylbenzene		8.77	8.77	6.0	1.8E-03
		p-xylene		8.44	8.47	7.0	1.4E-04
		1,3,5-cyclooctatriene		7.90	7.91	5.5	1.0E-05
108	C_7H_8O	benzyl alcohol		8.26	8.25	6.5	4.0E-04
115	C_9H_7	indenyl radical		7.48 [h]	7.56	8.0	1.5E-04
116	C_9H_8	1-ethynyl-4-methylbenzene	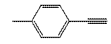	8.48	8.50	8.0	5.9E-04
		indene		8.14	8.18	7.5	8.0E-04
118	C_9H_{10}	indane		8.54 [g]	8.45	7.0	6.6E-05 [d]
	C_8H_6O	2-ethynylphenol		8.50			
		benzofuran		8.36			
122	$C_{10}H_2$	decapentayne		8.82 [f]	8.87	9.0	1.4E-05
126	$C_{10}H_6$	1,4-diethynylbenzene	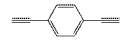	8.58	8.54	8.0	2.6E-04
128	$C_{10}H_8$	naphthalene		8.14	8.18	8.0	7.0E-04
130	C_9H_6O	inden-1-one		8.67 [g]	8.63	5.5	3.4E-05 [d]
	$C_{10}H_{10}$	2-butynylbenzene	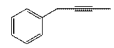	8.60			
		dialin		8.14	8.06	7.0	3.1E-05 [d]
		(E)-1-phenyl-1,3-butadiene	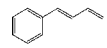	8.06			
		3-methylindene		7.97			
132	$C_{10}H_{12}$	3-butenylbenzene	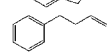	8.60	8.66	5.5	1.3E-05
		(E)-1-phenyl-1-butene	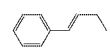	8.00	7.95	7.0	5.5E-06 [d]
		2-ethenyl-1,4-dimethyl-benzene		8.00			
140	$C_{11}H_8$	2-ethynyl-1H-indene	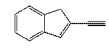	8.04	8.02	8.0	1.8E-04 [d]
		1H-cyclopropa[b]naphthalene		8.03			
142	$C_{11}H_{10}$	1-methylnaphthalene		7.96	7.87	7.0	1.3E-04 [d]
		2-methylnaphthalene		7.91			
144	$C_{11}H_{12}$	1,2,3,4-tetrahydro-1-methylene-naphthalene		7.90	7.84	6.5	3.5E-05 [d]
	$C_{10}H_8O$	2-naphthalenol	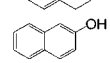	7.87			
		1-naphthalenol		7.76			

Table 2. Countinued

Mass	Formula	Species: Name	Species: Chemical Structure	IE (eV): Literature[a]	IE (eV): Measured[b]	Mole Fraction: Peak Position (mm)	Mole Fraction: X_{MAX}
150	$C_{12}H_6$	1,2-dehydroacenaphthylene		8.53[g]	8.52	8.5	3.6E-05
152	$C_{12}H_8$	acenaphthylene		8.12	8.10	8.0	4.7E-04[d]
		2-ethynylnaphthalene	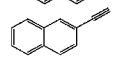	8.11			
		biphenylene	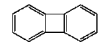	7.58	7.49	8.0	2.2E-05
154	$C_{12}H_{10}$	biphenyl	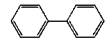	8.16	8.22	8.0	1.0E-04
		acenaphthene		7.75	7.71	6.5	8.5E-06[d]
		1-ethenylnaphthalene		7.70			
156	$C_{12}H_{12}$	1,4-dimethylnaphthalene		7.78	7.80	6.0	5.0E-05
166	$C_{13}H_{10}$	fluorene	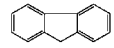	7.91	7.89	7.5	1.6E-04
168	$C_{13}H_{12}$	diphenylmethane	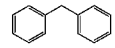	8.55	8.61	7.5	5.5E-05
		2-methylbiphenyl	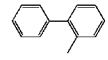	8.10	8.04	7.0	5.8E-05
176	$C_{14}H_8$	1,8-diethynylnaphthalene		7.88	7.87	8.5	1.2E-04
178	$C_{14}H_{10}$	phenanthrene		7.89	7.90	8.0	5.1E-05
		anthracene	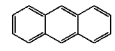	7.44	7.46	8.0	5.6E-05
180	$C_{14}H_{12}$	9,10-dihydrophenanthrene		7.55	7.51	7.0	3.4E-05
182	$C_{14}H_{14}$	bibenzyl	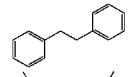	9.00	9.02	5.5	1.4E-05
		3,3'-dimethylbiphenyl	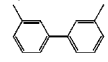	7.85	7.93	7.0	1.5E-05
190	$C_{15}H_{10}$	cyclopropa[b]anthracene	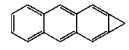	7.39	7.39	8.0	7.4E-05
192	$C_{15}H_{12}$	1-methylphenanthrene	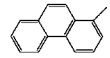	7.70	7.65	6.5	3.6E-05
202	$C_{16}H_{10}$	pyrene		7.43	7.47	8.0	6.8E-05
204	$C_{16}H_{12}$	2-phenylnaphthalene	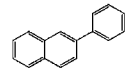	7.75	7.71	8.0	1.2E-05[d]
		1-phenylnaphthalene	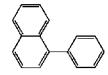	7.61[g]			
216	$C_{17}H_{12}$	benzo[c]fluorene	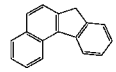	7.37[g]	7.31	8.0	2.8E-05[d]
		benzo[a]fluorene	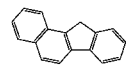	7.32[g]			
		benzo[b]fluorene	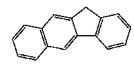	7.32[g]			
		7H-benzo[de]anthracene	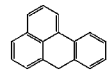	7.24[g]			

Table 2. Countinued

Mass	Formula	Species: Name	Species: Chemical Structure	IE (eV): Literature [a]	IE (eV): Measured [b]	Mole Fraction: Peak Position (mm)	Mole Fraction: X_{MAX}
228	$C_{18}H_{12}$	chrysene	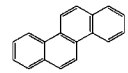	7.60	7.52	8.0	2.5E-06 [d]
		benz[a]anthracene	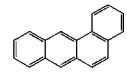	7.45			
240	$C_{19}H_{12}$	4H-cyclopenta[def]chrysene	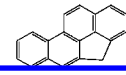	7.35 [g]	7.41	8.0	1.1E-05

[a] Ref 45 except for specific descriptions. [b] The errors of measured IEs in this work are ± 0.05 eV for species with strong S/N ratios and ± 0.10 eV for species with poor S/N ratios. [c] Ref 46. [d] The value is the total maximum mole fraction of the isomers with close IEs that are indistinguishable in this work, for example, the maximum mole fraction of 5.2×10^{-4} for $m/z = 76$ includes the contributions from benzyne and 3-hexene-1,5-diyne. [e] Ref 47. [f] Ref 48. [g] Calculated value in this work. [h] Ref 29.

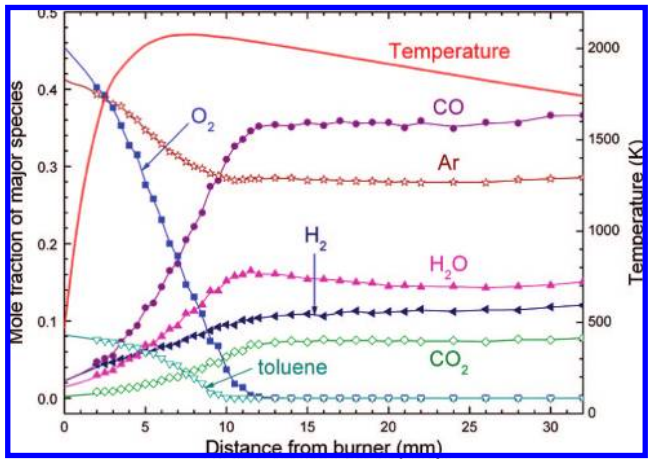

Figure 3. Mole fraction profiles of the major flame species (H_2, H_2O, CO, O_2, Ar, CO_2, and toluene) and the flame temperature profile.

carbon number, the peak position of mole fraction profile generally moves toward the burner surface with the increasing hydrogen number.

3.2.2. Primary Degradation Products of Toluene. There are some modeling studies concerning the degradation processes of small aromatic fuels like toluene and benzene in a jet-stirred reactor,[19] a flow reactor,[22] and premixed flames.[27,56] The common conclusion is that aromatic fuels will be attacked by active radicals, such as H, O, and OH radicals, leading to fuel destruction. In this work, the benzyl radical was observed with an extremely high concentration (reaching a maximum mole fraction of 1.2×10^{-3}) compared with other aromatic radicals; however, in the fuel-rich benzene flame studied by Yang et al.,[29] it could only reach a maximum mole fraction of 5.6×10^{-5}. These comparisons indicate the strong relation between benzyl formation and toluene degradation. Furthermore, no other isomer of the C_7H_7 radical could be observed in this work, even for the $C_6H_4CH_3$ radicals which were assumed as the phenylic H-abstraction product of toluene.[18,22] This phenomenon should be related to the fact that the benzyl radical has a much more stable molecular structure than the $C_6H_4CH_3$ radicals. Because of the resonant stabilization of the benzyl radical, its standard enthalpy of formation is 210.5 ± 4 kJ/mol,[57] which is quite lower than those of the $C_6H_4CH_3$ radicals (about 290 kJ/mol). Even if the $C_6H_4CH_3$ radicals can form in the flame, they are consumed quickly through either the oxidation by O_2, O, and OH or the isomerization to form the benzyl radical, leading to the low concentrations which are beyond the detection limit.

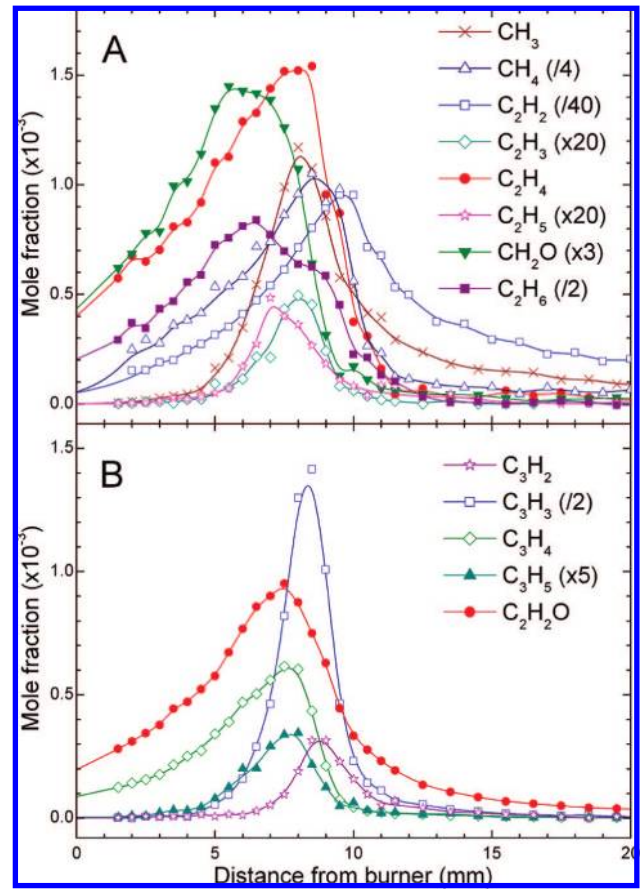

Figure 4. Mole fraction profiles of C_1- to C_3-species.

The dealkylation of toluene induced by H atom attack can lead to the formation of benzene, ($C_6H_5CH_3 + H = CH_3 + C_6H_6$), which was considered as an important channel of benzene formation in the stoichiometric methane doped toluene flame studied by El Bakali et al.[27] Besides, benzene can be produced through recombination reactions of its small precursors including the propargyl, allyl, C_4H_3, and C_4H_5 radicals, which have been considered to dominate benzene formation in the fuel-rich aliphatic hydrocarbon flames. To determine the dominant channel of benzene formation, we compared the maximum mole fractions of benzene and its precursors in this flame, the fuel-rich ethylbenzene flame,[42]

(56) Richter, H.; Howard, J. B. *Phys. Chem. Chem. Phys.* **2002**, *4*, 2038–2055.
(57) Hippler, H.; Troe, J. *J. Phys. Chem.* **1990**, *94*, 3803–3806.

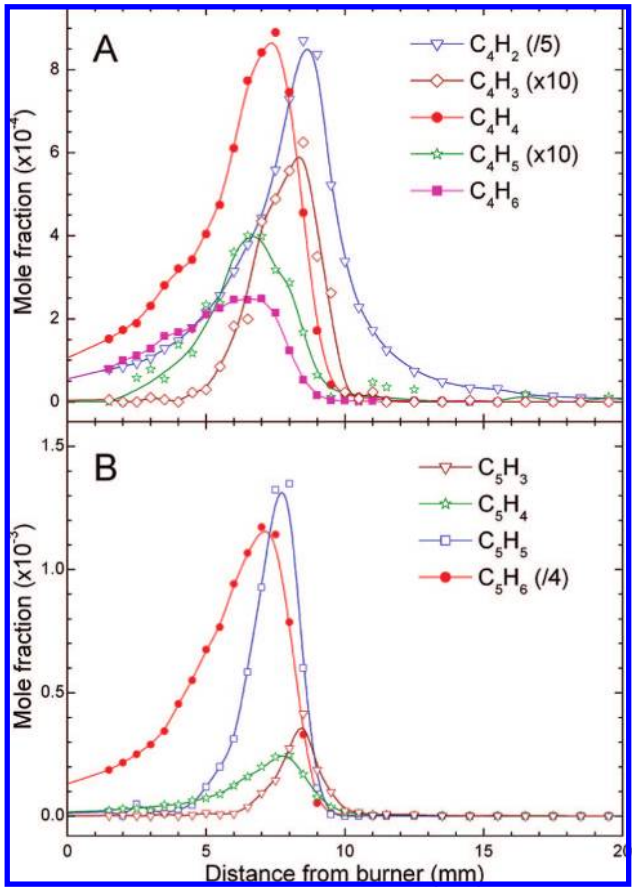

Figure 5. Mole fraction profiles of C_4- and C_5-species.

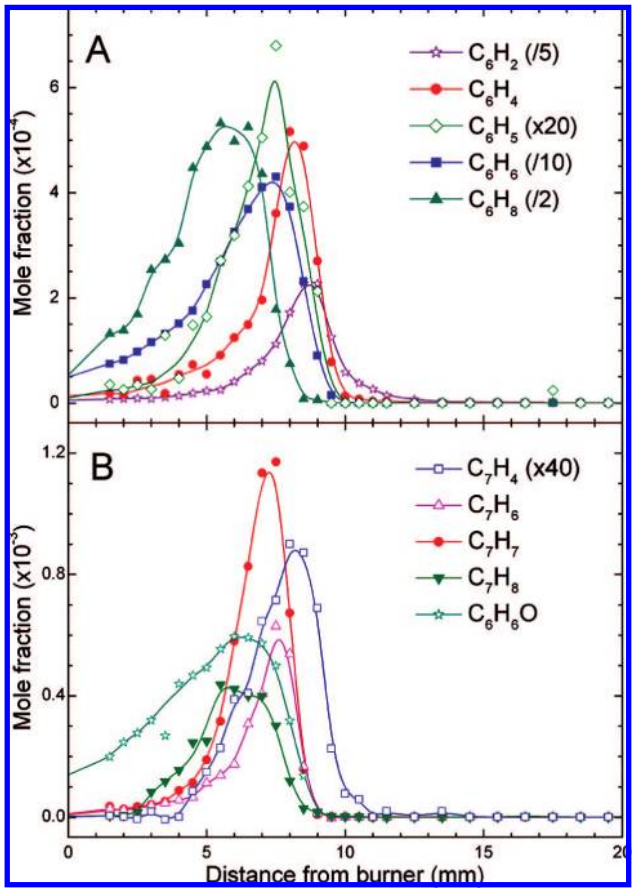

Figure 6. Mole fraction profiles of C_6-species and C_7-hydrocarbons.

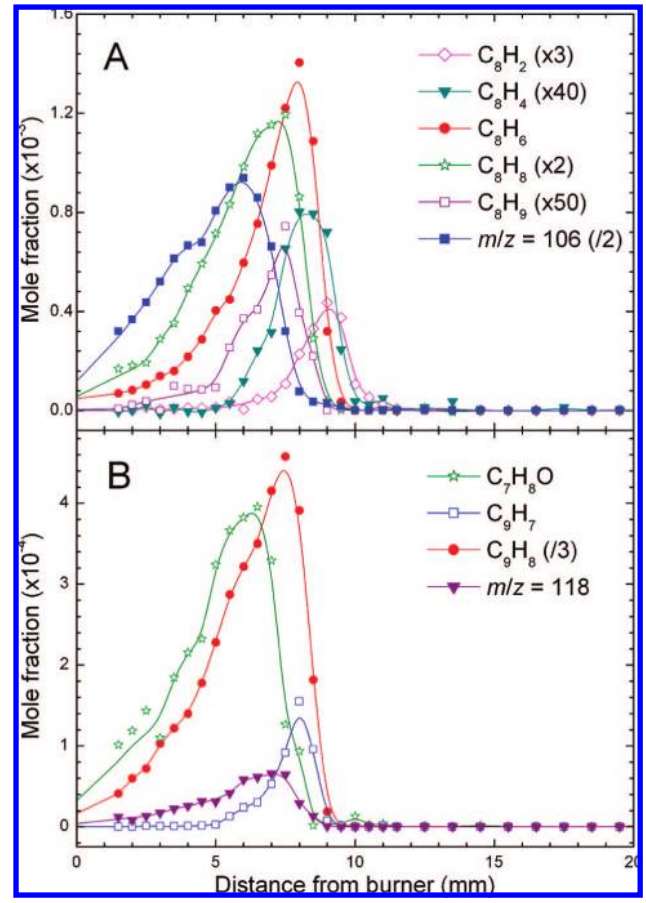

Figure 7. Mole fraction profiles of C_7H_8O, C_8- and C_9-species.

and several fuel-rich aliphatic hydrocarbon flames,[38,58,59] as listed in Table 3; the ratio of the most important precursor C_3H_3 and benzene is used to elucidate the role of small precursors for benzene formation in the aromatic hydrocarbon flames. It is noted that the C_3H_3/benzene ratios in the fuel-rich aliphatic hydrocarbon flames are around an order of magnitude higher than those in the fuel-rich aromatic hydrocarbon flames, implying the less contribution of C_3H_3 to benzene formation in the fuel-rich toluene and ethylbenzene flames. A similar situation also occurs for other small precursors as can be concluded from Table 3. Hence it is concluded that benzene is formed mainly through toluene degradation in this work.

Meanwhile, toluene can suffer some thermal decomposition processes and produce radical species such as the phenyl radical. But the major primary degradation products of toluene should be benzyl and benzene, both of which have maximum mole fractions exceeding 1×10^{-3}. Although both benzene and benzyl should appear in the low temperature region, say, before 5.0 mm, comparison between the mole fraction profiles of benzene and benzyl (Figure 6) shows that benzene can be formed in the low temperature region, and benzyl is produced mainly in the high temperature region. The low concentration of benzyl in the low temperature region should result from the high consumption rate of benzyl, for example, the benzyl oxidation to form benzaldehyde and the recombination of benzyl to bibenzyl. In particular, bibenzyl was found to appear at much

(58) Hansen, N.; Miller, J. A.; Taatjes, C. A.; Wang, J.; Cool, T. A.; Law, M. E.; Westmoreland, P. R. *Proc. Combust. Inst.* **2007**, *31*, 1157–1164.

(59) Kohse-Hoinghaus, K.; Oβwald, P.; Struckmeier, U.; Kasper, T.; Hansen, N.; Taatjes, C. A.; Wang, J.; Cool, T. A.; Gon, S.; Westmoreland, P. R. *Proc. Combust. Inst.* **2007**, *31*, 1119–1127.

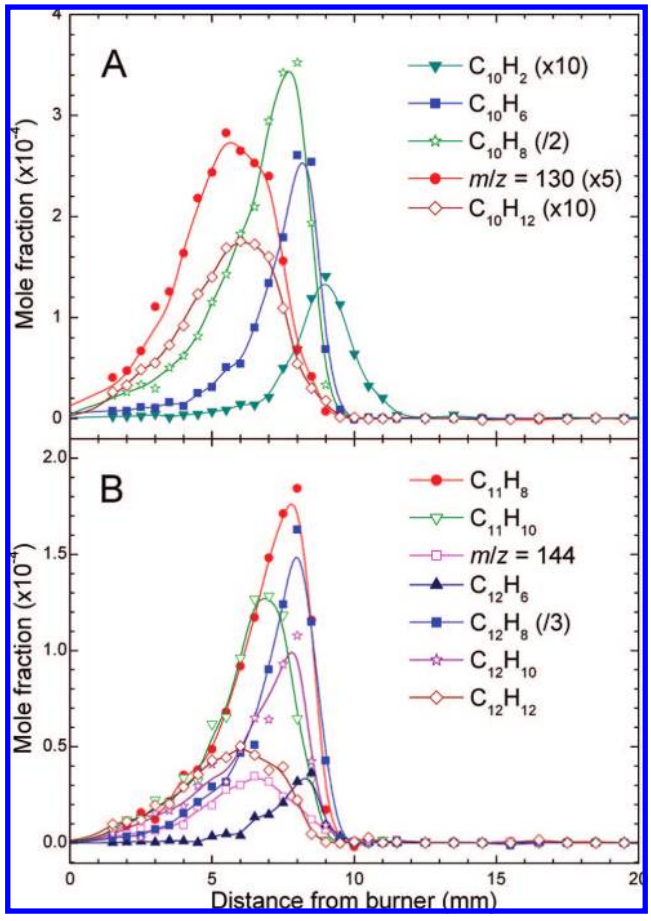

Figure 8. Mole fraction profiles of C_{10}- to C_{12}-species.

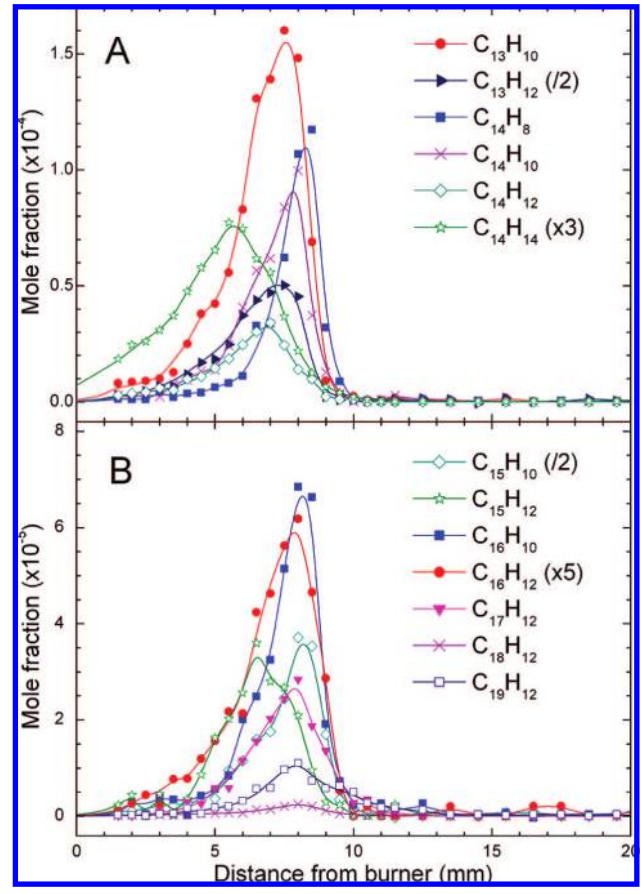

Figure 9. Mole fraction profiles of C_{13}- to C_{19}-species.

lower temperature than other products in the toluene pyrolysis.[24] Therefore in the low temperature region, these reactions consume most benzyl and promote the concentration levels of products such as bibenzyl and benzaldehyde, as seen from Figures 7A and 9A.

3.2.3. Large Monocyclic Aromatics, Polycyclic Hydrocarbons, and PAHs. Many large aromatics can be observed in this flame, including a series of monocyclic aromatics with more than 7 carbon atoms, polycyclic hydrocarbons, and PAHs. Here the species with at least two carbocycles, fused or unfused, are defined as polycyclic hydrocarbons, for example, benzocyclobutene, naphthalene, biphenylene, and so on. A series of polycyclic hydrocarbons which are composed of fused aromatic rings and do not contain heteroatoms or carry substituents have a common definition as PAHs.[60] Compared with those fuel-rich aliphatic hydrocarbon flames, this flame produces more abundant aromatic species (in both number and concentration) because of the benzenoid ring structure in the fuel molecule. In fact, the flame chemistry of aromatic fuels consists of two major categories; one includes the destruction and oxidation reactions to reduce the size of intermediates and produce final products, and the other part represents the molecular growth process to produce large aromatics. Hence, large intermediates with greater carbon numbers than the fuel definitely originate from the molecular growth process. For example, the formation of large aromatics can benefit from the combination of two intermediates or addition of a small linear intermediate to an aromatic intermediate.

(60) Fetzer, J. C. *Large (C> = 24) Polycyclic Aromatic Hydrocarbons: Chemistry and Analysis*; Wiley: New York, 2000.

Besides several C_1- or C_1/C_2-disubstituted and C_1/C_2-trisubstituted monocyclic aromatics like *p*-xylene, more than ten large monocyclic aromatics were detected in this work, which can be sorted as the C_2- and C_4-substituted monocyclic aromatics. Interestingly no C_3-substituted monocyclic aromatics can be observed. Even for the C_2- and C_4-substituted monocyclic aromatics, the concentrations of C_4-substitutes are generally 1 or 2 orders of magnitude lower than those of the C_2-substituted ones. All of the experimental observations ultimately lead to one conclusion, that is, aromatics with long aliphatic substituents tend to be unstable and less abundant in flame conditions, especially compared with those unsubstituted aromatics or aromatics with short aliphatic substituents. This conclusion can be supported by the observation that cyclization occurs even for those very stable C_2-substituted monocyclic aromatics. For example, benzocyclobutadiene, benzocyclobutene, and 1,3,5-cyclooctatriene were observed to coexist with phenylacetylene, styrene and ethylbenzene, respectively. Furthermore, this conclusion can explain why no C_3- and more-substituted PAHs and polycyclic hydrocarbons can be detected in this work.

The above discussion also implies that the ring growth process dominates the molecular growth process, which initiates from the formation of indene and naphthalene in combustion of monocyclic aromatic fuels. Lindstedt et al.[10] have outlined three major mechanistic channels for indene formation in their review, which are related to reactions of monocyclic radicals and small linear intermediates, that is, phenyl and C_3H_4 (allene/propyne), phenyl and propargyl, as well as benzyl and acetylene. All three channels seem to make sense in the fuel-rich monocyclic aromatic hydrocarbon flames, as the involved intermediates are all important ones. It was noticed that the indene concentration was found to be very sensitive to the benzyl concentration.[42] Therefore because of the high benzyl concentration, the reaction

Table 3. Comparison of the Maximum Mole Fractions of Benzene and Its Precursors among This Flame and Other Fuel-Rich Hydrocarbon Flames

	ethylene[38]	allene[58]	propene[59]	toluene	ethylbenzene[42]
ϕ	1.90	1.80	2.31	1.90	1.90
C/O	0.63	0.68	0.77	0.74	0.72
C_3H_3	4.3×10^{-4}	4.0×10^{-3}	3.4×10^{-3}	2.8×10^{-3}	3.9×10^{-3}
C_3H_5	6.8×10^{-5}		2.2×10^{-3}	6.9×10^{-5}	1.5×10^{-4}
C_4H_3	6.7×10^{-6}			6.3×10^{-5}	8.2×10^{-5}
C_4H_5	3.0×10^{-6}		6.9×10^{-5}	4.0×10^{-5}	1.2×10^{-4}
benzene	3.3×10^{-5}	6.5×10^{-4}	4.6×10^{-4}	3.9×10^{-3}	6.3×10^{-3}
C_3H_3/benzene	13.0	6.2	7.4	0.7	0.6

of benzyl and acetylene is suggested to dominate the indene formation in this flame.

On the basis of the intermediate identification and consequent comparison of the concentrations in this flame, the ring enlargement to produce naphthalene may occur via the reaction of acetylene and phenylacetylene, self-combination of cyclopentadienyl, and recombination of benzyl and propargyl, and so on. These channels are very representative since they belong to the common mechanisms relevant to PAHs formation. For instance, the reaction of acetylene and phenylacetylene belongs to the hydrogen-abstraction-carbon-addition (HACA) mechanism introduced by Frenklach and Wang,[61] which can be concluded as a repetitive sequence of two principal reaction steps, that is, (i) H-abstraction from the reacting hydrocarbon by a gaseous H atom, (ii) addition of acetylene to the radical site formed in step (i); the self-combination of cyclopentadienyl is an example of the five-member-ring recombination mechanism which considers the five-member-ring aromatics (fulvene, cyclopentadiene, and cyclopentadienyl) to represent important PAH precursors;[62] and the recombination of benzyl and propargyl represents another consideration that the propargyl radical can play an important role in the benzenoid ring formation and enlargement processes.[24,63] The last two mechanisms were always considered together as the odd-carbon mechanism or the resonantly stabilized radical addition mechanism since most of the major reactants are the resonantly stabilized radicals containing odd carbon atoms, such as the propargyl, cyclopentadienyl, and indenyl radicals. There are some other mechanisms such as the Diels−Alder mechanism which also considers acetylene as the key intermediate for ring growth but does not involve any radical species during the growth process,[64] the PAH isomerization mechanism (e.g., from phenanthrene to anthracene),[24,63] and the small substituted aromatics addition mechanism, for example, the addition of benzyl to toluene may lead to the formation of anthracene.[24,63] In a recent theoretical work, Kislov et al.[65] have shown that the Diels−Alder mechanism cannot compete with the HACA mechanism even at high combustion temperatures because of the large energy barriers. Moreover, the PAH isomerization mechanism and the small substituted aromatics combination mechanism are limited in scarce cases and cannot explain the sequential ring growth process.

For the HACA mechanism, five-member-ring recombination mechanism, and propargyl addition mechanism, there is still no definite conclusion for the dominant one in the molecular growth process to date. Actually, all of them can be bridges for the PAHs growth. For example, the five-member-ring recombination mechanism can connect indene to phenanthrene and benz[a]anthracene; and the HACA mechanism can connect benzene to naphthalene, and sequentially naphthalene to phenanthrene. Therefore we focus our attention on the question of how many observed species each mechanism can connect in this flame, which is similar to the question of how many piers a bridge has.

On the basis of the identification results of combustion intermediates in Table 2, a great deal of aromatic intermediates may benefit from the HACA mechanism during their formation process, even the dominant formation channel of indene, the reaction of benzyl and acetylene, is also part of a HACA channel; and the detailed reaction sequences are presented schematically in Figure 10. For example, the HACA reaction sequences can construct the molecular growth process from benzene to pyrene ($C_6H_6 \rightarrow C_8H_6 \rightarrow C_{10}H_6/C_{10}H_8 \rightarrow C_{12}H_8 \rightarrow C_{14}H_{10} \rightarrow C_{16}H_{10}$) and from benzyl to fluorene ($C_7H_7 \rightarrow C_9H_8 \rightarrow C_{11}H_8 \rightarrow C_{13}H_{10}$). It was commented that some HACA channels may encounter positive Gibbs free energy changes, resulting in the reverse shift of chemical balance.[66] Nevertheless in this flame, the high concentration of acetylene (reaching a maximum mole fraction of 3.8×10^{-2}) can drive these temperature-sensitive HACA channels to the forward side in the high temperature region and warrant the important role of the HACA mechanism in the molecular growth process.

For the five-member-ring recombination mechanism, the addition of a five-member ring will lead to the direct ring

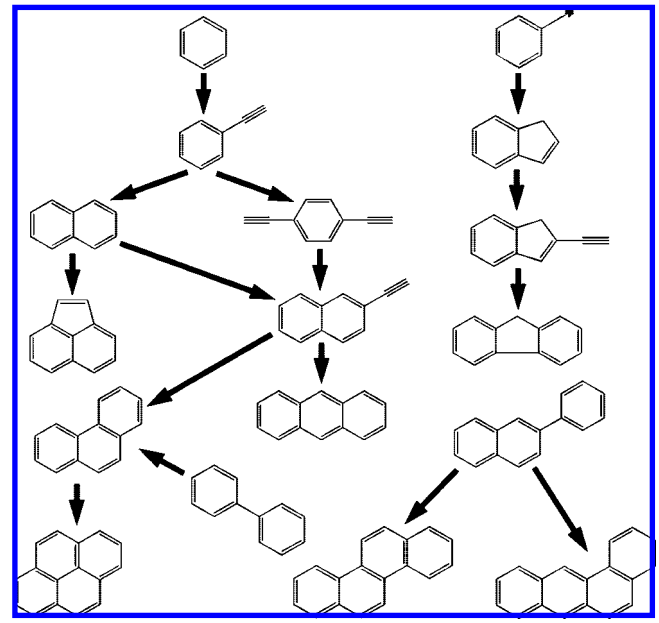

Figure 10. Molecular growth process related to the HACA mechanism in this work.

(61) Frenklach, M.; Wang, H. *Proc. Combust. Inst.* **1991**, *23*, 1559–1566.
(62) Melius, C. F.; Colvin, M. E.; Marinov, N. M.; Pitz, W. J.; Senkan, S. M. *Proc. Combust. Inst.* **1996**, *26*, 685–692.
(63) Colket, M. B.; Hall, R. J.; Smooke, M. D. *Mechanistic Models of Soot Formation*. United Technologies Research Center Report No. UTRC94-28, 1994.
(64) Siegmann, K.; Sattler, K. *J. Chem. Phys.* **2000**, *112*, 698–709.
(65) Kislov, V. V.; Islamova, N. I.; Kolker, A. M.; Lin, S. H.; Mebel, A. M. *J. Chem. Theory Comput.* **2005**, *1*, 908–924.
(66) Marinov, N. M.; Castaldi, M. J.; Melius, C. F.; Tsang, W. *Combust. Sci. Technol.* **1996**, *128*, 295–342.

enlargement process, for example, from cyclopentadiene/cyclopentadienyl (C5, carbon atom number in ring, regardless of the carbon atom number in the substituents) to naphthalene (C10), and indene/indenyl (C9) to phenanthrene (C14) or benz[a]anthracene (C18). For the propargyl addition mechanism, its role was generally emphasized in the benzene and naphthalene formation processes because of the few attentions on the C_1-substituted PAHs. Similarly to the propargyl self-combination, the propargyl attack on the C_1-substituted PAHs can form a new benzenoid ring, for example, from toluene/benzyl (C6) to naphthalene (C10), 3-methylindene (C9) to fluorene (C13), methylnaphthalenes (C10) to phenanthrene or anthracene (C14), and 1-methylphenanthrene (C14) to chrysene (C18). Therefore, combining the two mechanisms together, the resonantly stabilized radical addition mechanism can cover many typical PAHs observed in this work, such as indene, naphthalene, fluorene, phenanthrene, anthracene, and chrysene; but neither mechanisms explain the formation of so many ethynyl-substituted aromatics readily, and cannot be directly used to explain the regular ring enlargement by consecutive addition of 2 or 4 carbon atoms as the HACA mechanism does. Therefore it is concluded that the molecular growth process in this flame can result from the synergy of the HACA mechanism and the resonantly stabilized radical addition mechanism; that is, the HACA mechanism can cover more observed aromatic species, and the resonantly stabilized radical addition mechanism may have marked and sometimes predominant influences on the formation of many typical PAHs.

Conclusions

A premixed toluene/O_2/Ar flame with the equivalence ratio of 1.90 was investigated at 30 torr using tunable synchrotron VUV photoionization mass spectrometry. Combustion intermediates from $m/z = 15$ up to 240 were identified by the measurements of the photoionization mass spectrum and PIE spectrum. Mole fraction profiles of the flame species were determined from spatial signal profiles resulting from the scan of burner position at selected photon energies near ionization thresholds, providing information of the flame structure. Furthermore, flame temperature was recorded by a Pt/Pt-13%Rh thermocouple. On the basis of the experimental results, the fuel degradation and large aromatics formation are discussed in detail. The major primary degradation products of toluene are benzyl and benzene, which both have high concentrations in this flame. It is concluded that benzene is mainly produced via the fuel degradation instead of the radical recombination in the fuel-rich monocyclic aromatic hydrocarbon flames. Aromatics with long aliphatic substituents are found to be quite unstable in flame conditions compared with unsubstituted aromatics and aromatics with short aliphatic substituents. On the basis of the intermediate identification, comparison is made among the current PAH formation mechanisms. It is concluded that the molecular growth process in this flame should mainly result from the synergy of the HACA mechanism and the resonantly stabilized radical addition mechanism. In particular, the HACA mechanism can connect a great deal of observed aromatic intermediates and explain the regular ring enlargement by consecutive addition of 2 or 4 carbon atoms, while the resonantly stabilized radical addition mechanism may have marked and sometimes predominant influences on the formation of many typical PAHs.

Acknowledgment. F.Q. is grateful for the funding supports from Chinese Academy of Sciences, Natural Science Foundation of China under Grant 20533040, National Basic Research Program of China (973) under Grant 2007CB815204, and Ministry of Science and Technology of China under Grant 2007DFA61310. The authors are thankful for the valuable help in the experimental work from Mr. Taichang Zhang and Mr. Aiguo Zhu.

Supporting Information Available: Further details in two parts on "Mole Fraction Evaluation" and "Photoionization Cross Section". This material is available free of charge via the Internet at http://pubs.acs.org.

EF800902T